

A New VTOL UAV Cyclocopter with Cycloidal Blades System

Chul Yong Yun and Illkyung Park
cyyun@kari.re.kr, mechguy77@kari.re.kr

Research Engineer
Korea Aerospace Research Institute, Daejeon, Korea

Ho Yong Lee, Jai Sang Jung and In Seong Hwang
leehy@aeroguy.snu.ac.kr, deepli2@aeroguy.snu.ac.kr, ishis01@aeroguy.snu.ac.kr

Graduate Research Assistant
School of Mechanical and Aerospace Engineering, Seoul National University, Seoul, Korea

Seung Jo Kim
sjkim@snu.ac.kr

Professor
School of Mechanical and Aerospace Engineering, Seoul National University, Seoul, Korea

Sung Nam Jung
snjung@chonbuk.ac.kr

Associate Professor
Department of Aerospace Engineering, Chonbuk National University, Jeonju, Korea

ABSTRACT

The cycloidal blades system is a thrust propulsion system that consists of several blades rotating about a horizontal axis perpendicular to the direction of normal flight. In order to generate the thrust required, the pitch angles of the individual blades to the tangent of the circle of the blade's path are varied by a pitch control mechanism installed in the cycloidal blades system so designed that the periodic oscillation of the blades about their span axis may be changed both in amplitude and in phase angle. Therefore, the cycloidal blades system is able to vector its high thrust anywhere within a 360° arc parallel to the propellers plane of rotation. This characteristic enables the cycloidal blades system to take off and land vertically, hover and fly forwardly by simple adjustment of blades pitch angles.

INTRODUCTION

Recently, interests in an Unmanned Aerial Vehicle (UAV) increase as the UAV can gradually execute existing aviation mission functions in concert with or in lieu of manned systems. And UAV type shows a tendency to replace a fixed-wing UAV with a rotary-wing UAV according to the necessity to operate in various mission environments [1,2]. The rotary-wing UAV has advantages of the capability to approach the target point to hovering flight or low speed forward flight as well as to take off and land vertically. There are many rotary-wing UAV types such as a conventional helicopter type, coaxial contra rotor type, tilt rotor type, and ducted fan type. Among them, aircrafts with helicopter configurations are mainly used as UAV types capable of vertical take-off and landing

because of the experiences of successful manned helicopters. However, the UAV with helicopter type is limited in the forward flight speed due to rotating rotor, and the performance is also inferior to that of fixed-wing UAV in cruise flight. Therefore, many attempts were made to develop the rotary-wing UAV with both VTOL characteristics at take-off and landing and fixed-wing characteristics at forward flight such as CRW (Canard Rotor Wing) and tilt rotor. However, these rotors must overcome the instability problems occurring in transition mode from vertical flight to horizontal flight or from rotary wing to fixed wing.

A cyclocopter with the cycloidal blades system can be the type of UAV which can combine the high-speed characteristics of the conventional airplane with the low-speed characteristics of the helicopter. The cycloidal blades system, which can be described as a horizontal rotary wing, offers powerful thrust levels, and a unique ability to change the direction of the thrust almost instantly. In this paper, the characteristics of the cycloidal blades system and cyclocopter with

Presented at the American Helicopter Society 60th Annual Forum,

Baltimore, MD, June 7-10, 2004.

Copyright © 2004 by the American Helicopter Society International, Inc. All rights reserved.

this system are described.

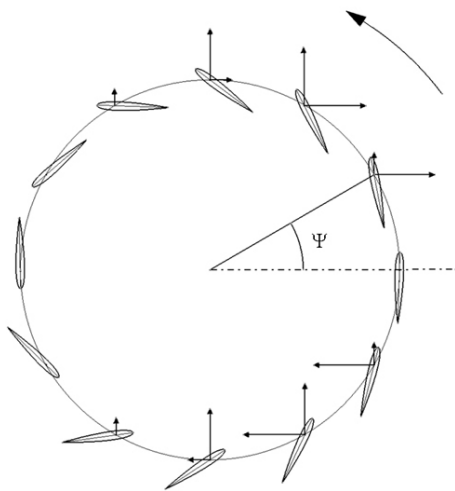


Fig. 1 Blade pitch angle variation during a revolution

The cycloidal blades system [3-8, 19] is a thrust propulsion system that consists of several blades rotating about a horizontal axis perpendicular to the direction of normal flight. In order to generate the thrust required, the pitch angles of the individual blades to the tangent of the circle of the blade's path are varied by a pitch control mechanism installed in the cycloidal blades system so designed that the periodic oscillation of the blades about their span axis may be changed both in amplitude and in phase angle. Therefore, the cycloidal blades system is able to vector its high thrust anywhere within a 360° arc parallel to the propellers plane of rotation. This characteristic enables the cycloidal blades system to vertically take off and land, hover and fly forwardly by simple adjustment of blades pitch angles. Fig. 1 shows typical pitch motion experienced by a blade on its rotating orbit. The blade on the top and the bottom positions produces upward force with positive angle of attack. On the other hand, the blade on the left and the right positions produces small amount of force, because the blade has little angle of attack.

Fig. 2 represents a diagram of composite velocities of a blade rotating about a center with constant rotating tip velocity at high speed forward flight. The resultant velocity on the blade is the vector sum of the tip velocity and advance velocity, the former being represented by a vector tangent to the orbit at the position of the blade. In high speed forward flight, the blade pitch motions with respect to azimuth angle during the rotation are that the leading edges of all the blades must be headed in the forward direction to produce the propulsion force and the lift as shown in Fig. 2. In this case, the pitch angle variation about feathering axis is high. Therefore, this pitch motion is

called high pitch motion which is suitable to high-speed forward flight. Fig. 3 shows the blade pitch motion and velocity component on the blades in low speed forward flight or hovering flight. The pitch motion of the blade occurs close to the tangent of the rotating orbit because the rotating velocity has a more effect on the resultant velocity than the advance velocity does. This pitch variation is low, so it is called low pitch motion.

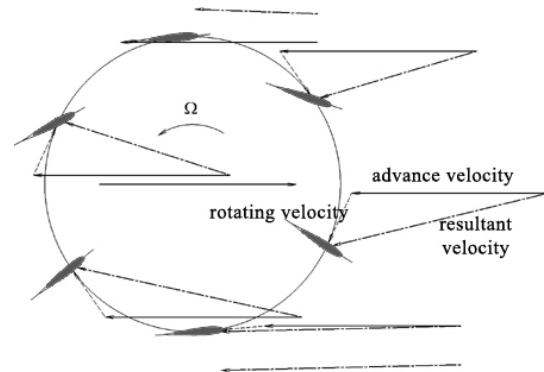


Fig. 2 Blade pitch motion and velocity components on a blade at high forward speed

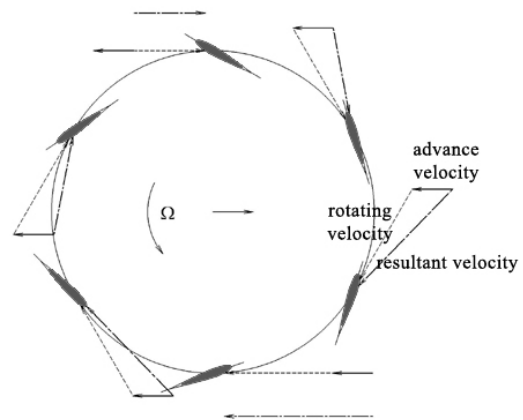


Fig. 3 Blade pitch motion and velocity components on a blade at low forward speed

In this paper, a cycloidal blades system operated in air are investigated in numerical and experimental manner to verify the characteristics and the performance of the system, and an unmanned aerial vehicle, named as a cyclocopter, installing this cycloidal blades system is designed and developed to evaluate the potential of cycloidal blades system for VTOL vehicle. This work is focused on the hovering and low speed forward flight of the vehicle.

AERODYNAMIC THEORY OF CYCLOIDAL BLADES SYSTEM

The momentum theory and the blade element theory are used for the derivation of an aerodynamic theory for the cycloidal blades system. Streamtube model can be used to predict the performance of the cycloidal rotor system. Streamtube theory was originally developed for the analysis of vertical axis wind turbines such as darrieus wind turbine [9]. In streamtube models the induced axial velocity is calculated at the rotor by equating the time-averaged force on the blades to the mean momentum flux through a streamtube of fixed location and dimensions. Aerodynamic forces are calculated from local angles of attack and local relative velocities. The theory assumes that there are two actuator disks in tandem at the upstream and downstream blades passes. Hence, the theory allows for variation in the induced velocities at each circumferential position as the blade rotate [10,11]. However, the method is not accurate at hovering and low advance ratios since the induced flow does not pass straightly, but is bent at the actuator disks in real world. In this section, double-multiple streamtube model will be modified to consider bent induced flow and flow curvature to improve the predicting accuracy of the cycloidal rotor performance.

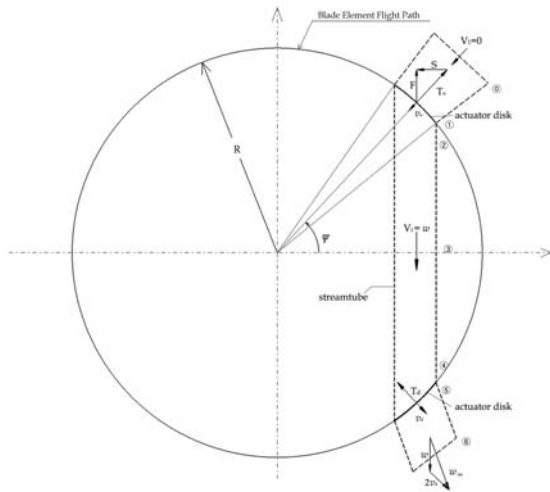


Fig. 4 Flow model used for momentum theory analysis of a cycloidal rotor in hover

Momentum theory

In the model, it is assumed that the cycloidal blades system can be represented by a pair of actuator disks in tandem as stated previously. This analytical method uses a multiple-streamtube model divided into two parts: one for the upstream half-cycle of the rotor and the other for the downstream half-cycle. As depicted in

Fig. 4, each streamtube intersects the blades' path twice, once on the upstream pass, and again on the downstream pass. At these intersections we imagine the rotor replaced by a tandem pair of actuator disks, upon which the flow may exert a force.

Upstream half of the rotor

In the general approach to the problem, it will be assumed that the flow through the rotor is one dimensional, quasi-steady, incompressible, and inviscid. Cycloidal rotor is idealized as an infinitesimally thin actuator cylinder over which a pressure difference between inner and outer surface exists. The actuator disk perpendicular to the generated thrust is capable of imparting axial momentum. It is assumed that the flow passes into the rotor in the normal direction to the tangential line of actuator cylinder and is deflected across the actuator cylinder to the downward direction so that the streamtube is bent as shown in Fig. 4. Hence, the rotor is split up into streamtubes and the induced velocities at the blades on the upstream and downstream actuator disks are found at each streamtube. It is also assumed that the free stream pressure is attained at some point inside the rotor and the velocity at that point is taken as the wake velocity for the upstream actuator disk and the free stream velocity for the downstream actuator disk.

From the momentum conservation and the energy conservation in the each stream tube shown in Fig. 4, a relationship between the induced velocity in the plane of the rotor and the far downstream in the rotor is as follows.

$$v_u = \frac{1}{2} w \sin \psi \quad (1)$$

Also the element thrust can be written as

$$dT_u = 2\rho R \left(\frac{v_u}{\sin \psi} \right)^2 d\psi \quad (2)$$

Downstream half of the rotor

For the upstream half-cycle of the rotor, the local flow velocity and far downstream velocity are v_u and w , respectively. For the downstream half-cycle of the rotor, the far downstream velocity of the upstream half, w is considered as the far upstream (Fig. 4). The induced velocity in this part of the rotor, v_d is a function of far downstream velocity, w and the position, ψ . Applying the momentum conservation and the energy conservation to the lower actuator disk, the element thrust produced is

$$\begin{aligned} dT_d &= 2\dot{m}v_d \\ &= 2\rho R v_d \sqrt{w^2 + 2wv_d \sin \psi + v_d^2} d\psi \end{aligned} \quad (3)$$

Blade element theory

The blade element theory forms the basis of rotor aerodynamic analysis because it provides estimates of the azimuthal distributions of blade aerodynamic loadings. The blade element theory assumes that each blade section acts as a quasi-two-dimensional airfoil to produce aerodynamic forces [12].

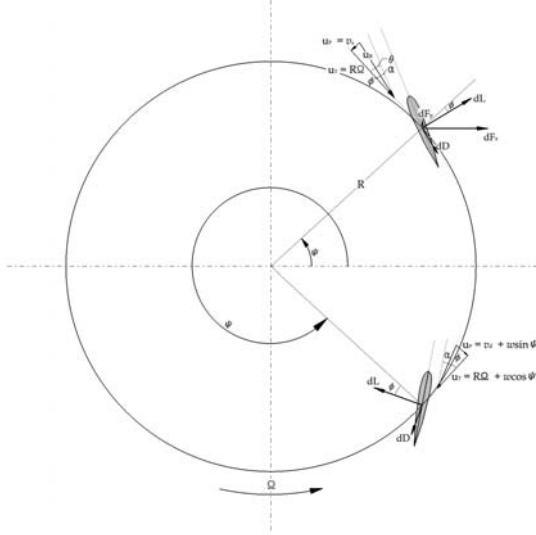


Fig. 5 Flow environment and aerodynamic forces

Upstream half of the rotor

Fig. 5 shows a sketch of the flow environment and aerodynamic forces at representative blade element on the rotor. The aerodynamic forces are assumed to arise solely from the velocity and angle of attack normal to the leading edge of the blade section. The induced angle of attack, ϕ arises because of the velocity induced by the rotor.

The resultant local flow velocity at any blade element has a perpendicular component $U_p = v_u = \lambda R\Omega$ normal to the rotor as a result of induced inflow and a tangential component $U_T = R\Omega$ parallel to the rotor because of blade rotation. The resultant velocity at the blade element is, therefore,

$$U_R = \sqrt{U_T^2 + U_p^2} \quad (4)$$

The relative inflow angle at the blade element will be

$$\phi = \tan^{-1}\left(\frac{U_p}{U_T}\right) \quad (5)$$

Thus, if the pitch angle at the blade element is θ , then the effective angle of attack is

$$\alpha = \theta - \phi \quad (6)$$

For a rotor with N_b identical blades, each of N_b blade elements spends $d\psi/2\pi$ percent of their time in the streamtube. Therefore the resultant incremental lift dL and drag dD per unit span on this blade element are

$$dL = \frac{1}{2} \rho U_R^2 \left(\frac{N_b d\psi}{2\pi} \right) c C_l \quad (7)$$

$$dD = \frac{\rho N_b c}{4\pi} U_R^2 C_d d\psi \quad (8)$$

where C_l and C_d are the lift and drag coefficients, respectively. The lift dL and drag dD act perpendicular and parallel to the resultant flow velocity, respectively. The quantity c and a are the blade chord and lift curve slope, respectively. N_b is the number of blades comprising the rotor.

Therefore, the thrust in the upper part of the rotor is

$$dT_U = dL \cos \phi - dD \sin \phi \quad (9)$$

Equating the incremental thrusts from the momentum and blade element theories (equations (2) and (9)) one finds that

$$4\kappa_{emp} \lambda^2 = \sigma a (1 + \lambda^2) \left\{ (\theta - \phi) \cos \phi - \frac{C_d}{a} \sin \phi \right\} \sin^2 \psi \quad (10)$$

where κ_{emp} is an empirical factor to cover non-uniform flow, 3-D effects, tip losses, etc. In this calculation, a value of 1.15 for κ_{emp} is used.

Downstream half of the rotor

For the downwind half of the rotor, $\pi \leq \psi \leq 2\pi$, the far downstream velocity, w , given by equation (1) is considered as the input condition of the flow in the downstream region at each streamtube. From Fig. 5, the perpendicular component and the tangential component of the resultant local flow velocity at any blade element for downstream half of the rotor are given by

$$U_T = R\Omega + w \cos \psi, \quad U_p = w \sin \psi + v_d \quad (11)$$

Using the blade element theory and the momentum equation (3) for each streamtube and equating the incremental thrusts, it is found that

$$4(\lambda - \zeta \tan \psi) \sqrt{\lambda^2 + \zeta^2} = \sigma \left\{ (1 + \zeta)^2 + \lambda^2 \right\} \left\{ a(\theta - \phi) \cos \phi - C_d \sin \phi \right\} \quad (12)$$

where $\lambda = (w \sin \psi + v_d) / R\Omega$ and $\zeta = w \cos \psi / R\Omega$.

Induced velocities

In the previous sections, the induced velocities for the upstream rotor and downstream rotor are found in the equations (10) and (12). The equilibrium-induced velocity, w , in the horizontal plane is also calculated using the equation (1). Fig. 6 shows a typical induced flow field of the cycloidal rotor. In the upstream part of the rotor, the inflow passes into the rotor in the normal direction. As shown in the figure, the inflow speed is zero at azimuth angle of 0° and 180° . The maximum speed of inflow appears at $\psi = 90^\circ$. The flow speed increase as azimuth angle increase up to 90° . After this angle, the flow passes slowly. The flow pattern is symmetric about vertical axis. In the downstream part of the rotor the total flow through the rotor flight path is composed of the component of the equilibrium-induced velocity w , and the induced velocity v_d . In Fig. 6, it can be seen that the flow is tilted slightly with respect to the vertical axis though the phase angle of eccentricity is set to be zero. The axisymmetry of the flow through the downstream rotor is lost. This phenomenon can also be illustrated in the computation flow analysis described in later section.

Fig. 7 shows the induced flow velocity with respect to azimuth angle under the condition of the specific pitch angle and rotating speed. In the sign convention, when the flow is entering the rotor, the flow is positive in the sense. In turn, when the inflow velocity points out of the rotor, the flow is negative. The induced flow v_d in the region of $180^\circ < \psi < 270^\circ$ in downstream half of the rotor is entering the rotor as shown in Fig. 7 while in $270^\circ < \psi < 360^\circ$ the flow is leaving the rotor as expected. The magnitude of the flow velocity in the downstream rotor is smaller than that in the upstream.

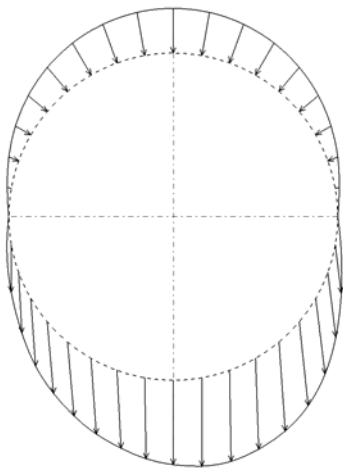


Fig. 6 Typical inflow distributions on the rotor

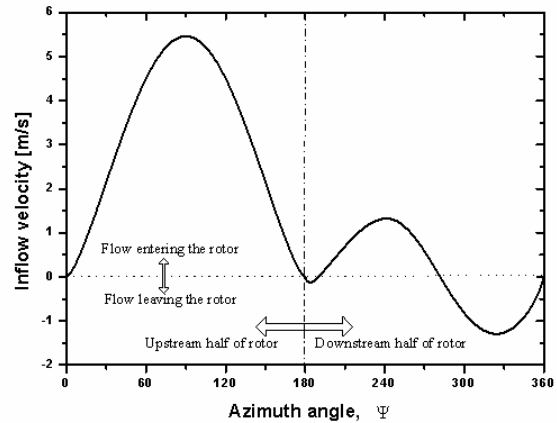


Fig. 7 The induced flow speed as a function of azimuth angle

Virtual Camber Effect

The aerodynamic theory in the previous section is based on the assumption that the inflow velocity and the incidence angle between the inflow and the chord line are constant along the chord of a blade. The peculiar aerodynamic characteristics associated with the orbital motion of the blades is that these blades are subjected to a curvilinear flow and behave very differently than if they were immersed in a rectilinear flow [13,14]. The local inflow velocity and angle of attack of the blades are unique everywhere on the chord. Thus, the blades have different aerodynamic characteristics from that of the symmetric blades though the blades are symmetric.

The local pitch angles depend on the ratio of chord to radius. The flow curvature effects become more pronounced as c/R increases. The rotor rotation causes the blade to behave like the cambered airfoil. The lift coefficient variations with respect to blade azimuth angle were examined for a blade of $c/R = 0.375$ with camber effect or without camber effect as shown in Fig. 8. It is assumed that there is no inflow entering and leaving the rotor. For the both cases, the lift coefficient varies to the sine curve form. However, the lift coefficient curve for the blade with camber effect is shifted to the down direction by approximately 0.5 comparing to that without camber effect. This explains that more amount of lift force is generated in the downstream part than in the upstream part. Fig. 9 shows the vertical force coefficient variation for a blade with camber effect or without camber effect. For the case without camber effect, the force is symmetric about horizontal axis and vertical axis of the rotor. It can be also seen that the vertical forces decrease in the upstream part and increase in the downstream part for a blade with camber effect. The horizontal force curve seems to be somewhat complex as shown in Fig. 10.

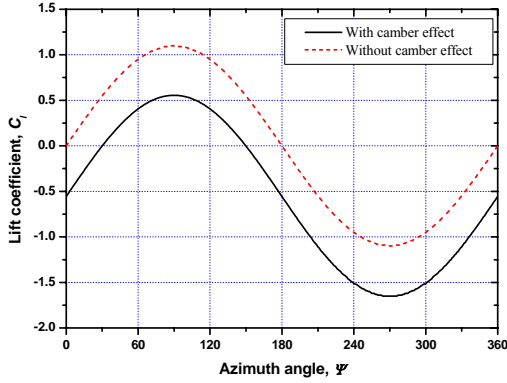


Fig. 8 Lift coefficient variations as a function of blade azimuth angle for the blade with camber effect or without camber effect

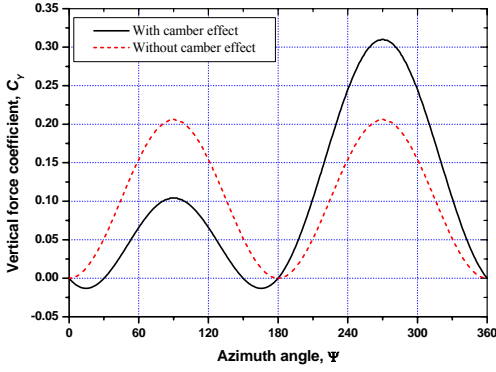


Fig. 9 Vertical force coefficient variations as a function of blade azimuth angle

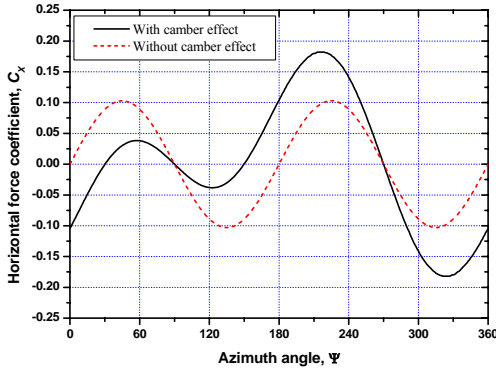


Fig. 10 Horizontal force coefficient variations as a function of blade azimuth angle

Force and Power on a Rotor

Up to this point, the instantaneous blade lift, moment and drag per unit span as a function of azimuth angle

have been derived for the forces on only one blade. The aerodynamic forces and moment for the rotor span can be calculated to be integrated along the blade from the root to the tip. The lift L and drag D act perpendicular and parallel to the resultant flow velocity, respectively. These forces can be resolved radial and tangential to the blade element flight path giving

$$\begin{aligned} F_R &= L \cos \phi - D \sin \phi \\ F_T &= L \sin \phi + D \cos \phi \end{aligned} \quad (13)$$

In order to obtain the total thrust produced on a rotor by all the blades, the resolution of the radial and tangential forces into horizontal force F_x and vertical force F_y components results in the equations

$$F_X = \frac{N_b}{2\pi} \int_0^{2\pi} (F_R \cos \psi + F_T \sin \psi) d\psi \quad (14)$$

$$F_Y = \frac{N_b}{2\pi} \int_0^{2\pi} (F_R \sin \psi - F_T \cos \psi) d\psi$$

where N_b is the number of blades.

The total thrust produced on a cycloidal rotor becomes

$$T = \sqrt{F_X^2 + F_Y^2} \quad (15)$$

The torque about the axis of rotation results from the tangential force which is composed of the profile drag and the induced drag. And there is additional torque arising from maintaining the oscillation of the blade per revolution. Hence, the expression of the total torque of a rotor is

$$Q = \frac{N_b}{2\pi} \left(\int_0^{2\pi} R F_T d\psi - \frac{M \dot{\alpha}}{\Omega} \right) \quad (16)$$

where M is aerodynamic moment. Above the equation, the minus sign is adopted since the moment is positive when the blade is in nose-up state.

Therefore, the power required to turn the blades can be obtained by the following equation.

$$P = Q\Omega \quad (17)$$

CFD ANALYSIS

CFD analysis was used to determine the aerodynamic design parameters of cyclocopter rotor system. CFD analysis offers not only the thrust prediction of cyclocopter rotor, but also understanding flow conditions around rotor and blades that are not observed through analytic and experimental method. To simulate rotating and pitching motion of blade, the moving mesh method is used in CFD analysis. As well

as, to improve the accuracy of CFD results, the CFD models of CBS(Cycloidal Blades System) test apparatus are generated and the results of CFD analysis are compared with results of CBS test apparatus.

CFD model for CBS apparatus

The CBS test apparatus is a device made for the purpose to verify VTOL capability and hovering performance. Therefore, the size of solution domain and boundary conditions of the CFD model for the CBS test apparatus are made so that it is suitable to this purpose and it is illustrated in Fig. 11. And the $k - \epsilon$ /Low Reynolds turbulence model is applied on the CFD model as turbulence model, and structured and unstructured meshes are used in the CFD model of CBS test apparatus. Meshes in CFD model of CBS test apparatus are presented in Fig. 12.

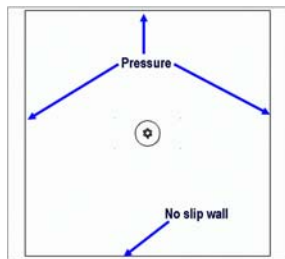


Fig. 11 The imposed boundary conditions

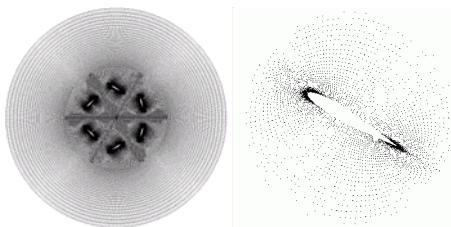


Fig. 12 Meshes in the CFD model

Results of CFD analysis of CBS test apparatus

Fig. 13 shows that the air is induced into the CBS rotor by rotating blades. The induced airflow occurred by rotating blades flows into the CBS rotor in the normal direction through the semi circle, and then this induced airflow after passing the semicircle is in a downward direction of the CBS rotor. Fig. 14 shows the outflow of the CBS rotor. The outflow of the CBS rotor is refracted about 20° after passing downside blades. The refraction of the airflow of the CBS rotor is induced by the inner airflow of the CBS rotor. The inner airflow increases the resultant velocity of the right and down side blades with $270^\circ < \Psi < 360^\circ$, on the other hand it decreases the resultant velocity of the

left and down side blades with $180^\circ < \Psi < 270^\circ$. Therefore, the non-symmetry downstream is occurred, and the refraction of the outflow of the CBS rotor is developed. Fig. 15 presents the streamline of the airflow of the CBS rotor.

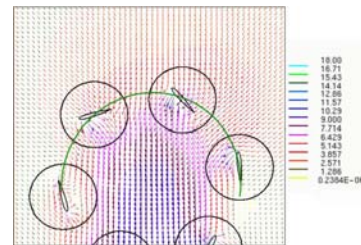


Fig. 13 Induced airflow into the CBS rotor

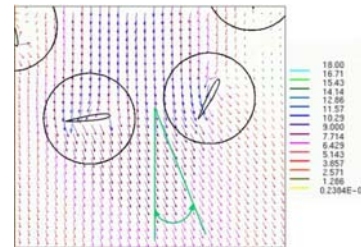


Fig. 14 Outward airflow from the CBS rotor

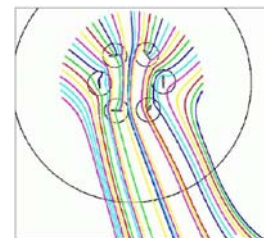


Fig. 15 Airflow around the CBS rotor

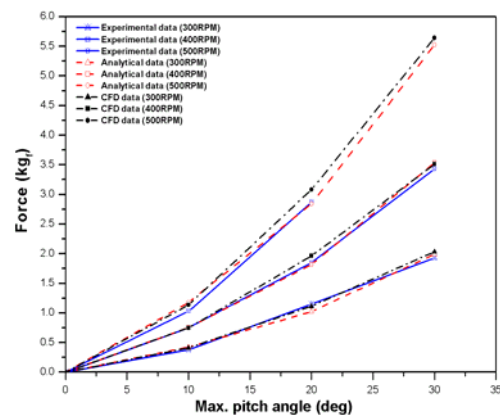


Fig. 16 Comparison CFD results with analytic results and experimental results

Fig. 16 illustrates the comparison of the results obtained from CFD analysis to the analytic and experiment results. The experimental results for comparison refer to the reference [15]. Despite difference of the thrust from the experimental results increases with respect to rotating speed, the comparison in Fig. 16 shows to us that the CFD analysis can predict the thrust of the CBS rotor very well.

EXPERIMENT OF CYCLOIDAL BLADES SYSTEM

In this section, experimental study for cycloidal blades system will be described to examine its performance. Experimental apparatus was constructed for cycloidal blades system rotating about horizontal axis. In the experiment for cycloidal blades system, the cycloidal blades system is designed and implemented with sinusoidal low pitch system to investigate the fundamental characteristics in hovering state. The main key component of this apparatus is rotating blades, which generate the thrust. The experimental test model is mainly composed of rotor blades, transmission device for the blades rotating, thrust control mechanism capable of varying the magnitude and direction of thrust vector, and measuring units for the thrust and power.

Rotor blades

Rotor blades are designed to withstand relatively high transverse centrifugal loadings, and responding to a number of aerodynamic harmonic vibratory forcing frequencies. To reduce the weight and increase the strength, the blades are made of composite materials. The blades consist of the skin, spar, and trailing stiffener.

Sinusoidal low pitch system

For a cycloidal blades system the rotor is unique because, unlike a propeller, it must provide both a lifting force and a propulsive force. It can be done by varying the pitch angle of the individual blades in a periodic manner with respect to azimuth angle during the rotation. A pitch bearing is incorporated into the blade to allow the blades to feather, providing an ability to change their pitch. This can be done by control block motion in a translation manner, thereby changing the magnitude of the rotor thrust, or in a rotation manner, thereby changing the phasing of the aerodynamic loads, which allows the rotor control block to tilt so as to reorient the rotor thrust vector. The pitch angle is varied like a sine curve with respect to azimuth angle. Blade pitch motion can be done by

means of a control block.

The magnitude of eccentricity e is defined as the distance from the center of rotation O to the point of the eccentricity point P as shown in Fig. 17. The phase angle of eccentricity ε is defined as the angle between the line OP and the vertical line. The magnitude and the phase angle of the eccentricity are used to adjust the magnitude and the direction of the thrust generated in this system.

Referring to Fig. 18, the pitch angle in sinusoidal low pitch system in terms of magnitude, phase angle and azimuth angle is written as

$$\theta = \frac{\pi}{2} - \cos^{-1}\left(\frac{a^2 - L^2 + p^2}{2ap}\right) - \sin^{-1}\left(\frac{e}{a}\cos(\psi + \varepsilon)\right) \quad (18)$$

where a is the distance from the eccentricity to the pivot point of a blade given by $a = \sqrt{e^2 + R^2 + 2eR\sin(\psi + \varepsilon)}$ and p is the distance from the pivot point to the connection point between a control rod and the blade, and L is the length of the control rod.

The pitch angle variation of each blade in the low pitch system according to azimuth angle is shown in Fig. 19. The phase angle and the magnitude of the eccentricity are set to be zero and $0.05R$, respectively. The pitch angle variation is similar to the sine curve. Therefore this low pitch system is called sinusoidal low pitch system. Since the pitch angle is varied like sine curve, the pitch angle will be assumed to be a sinusoidal function of ψ , and the instantaneous pitch angle θ can be expressed as

$$\theta = \theta_a \sin(\psi + \varepsilon) \quad (19)$$

where θ_a is amplitude of pitch angle for varying angles. Above equation is used to calculate the aerodynamic loads for cycloidal blades system.

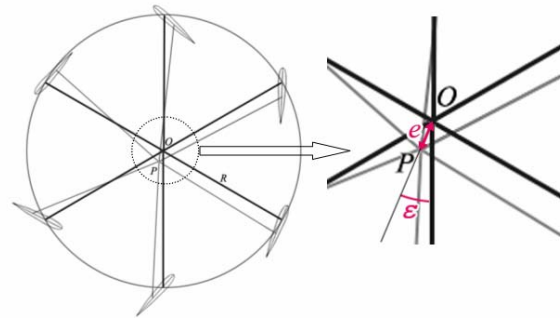


Fig. 17 Sinusoidal low pitch systems

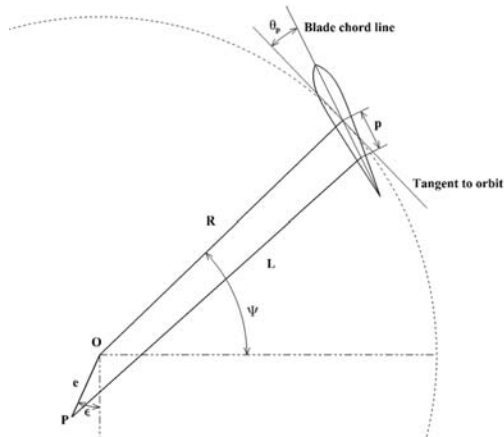


Fig. 18 Geometry for the blade pitch angle and eccentricity

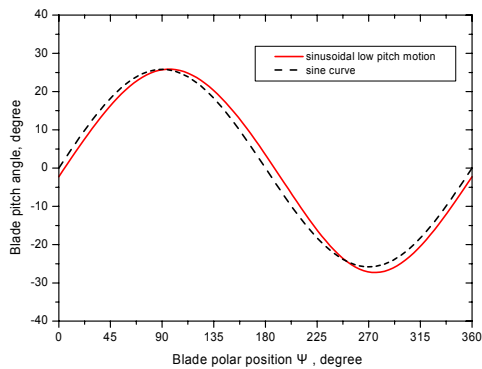


Fig. 19 The pitch angle variation as a function of azimuth angle

Experimental tests of cycloidal blades system

The rotor model tested is a six-bladed rotor with a diameter of 0.4m as a baseline configuration. The span and chord of the blade are 0.8m and 0.15m, respectively. The airfoil section used in blade is NACA 0012. Fig. 21 shows an overall view of the cycloidal blades system. The height of rotor shaft is 1.432m from the ground. The test model consists of main stand, auxiliary support and one cycloidal rotor driven by a motor. The rotor system is powered by a 1.5 kW AC servo motor. Power of the motor is transmitted through a timing belt into the main shaft [16].

A radius of rotor can be changeable to 0.45m or 0.5m though the radius of rotor in baseline configuration is 0.4m. The hub arm which connects each blade with main shaft has 4 sets of bolt-hole position so that the rotor radius can be varied by altering these connection levels. Also, the model can be a two-bladed or three-bladed rotor as well as a six-bladed rotor. The pitch angles of blades can be varied continuously by control mechanism. The amplitude of

pitch angle changed cyclically per revolution reaches maximum 35° . The ranges of parameters capable of adjusting in the test are shown in Table 1.

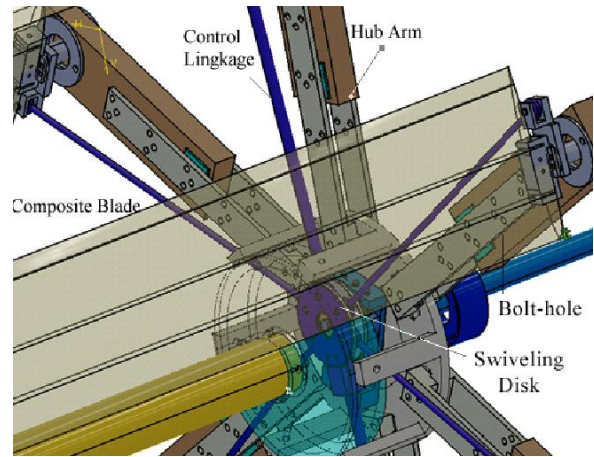


Fig. 20 Design of rotor with control device



Fig. 21 Test model of cycloidal blades system

Table 1 Experiment test variables

| Parameter | Range |
|--|-------------------------|
| Number of blade, N_b | 2, 3, 6 |
| Rotational velocity, Ω | 0 ~ 600 RPM |
| Amplitude of pitch angle, θ_a | $0^\circ \sim 35^\circ$ |
| Rotor radius, R | 0.4m, 0.45m, 0.5m |
| Phase angle of eccentricity, ε | $-70 \sim +110^\circ$ |

Experimental results

In this section, the experimental results will be described to examine the effects of the various rotor parameters. The performance for the baseline

configuration of cycloidal blades system will be presented at first. Next, the others configuration will be going on. For the baseline configuration, analytical results obtained from the aerodynamic theory model will be compared with the experimental results.

At first, the test runs under the condition that the blades are removed from the rotor are made to measure the power consumed by hub arms and mechanical loss. The test results for the rotor power in this paper are obtained by subtracting from the gross or measured power on the rotor the power obtained with the blades removed.

Baseline configuration

At first, the tests for the baseline configuration are conducted to identify the performance and the effects of the magnitude and direction of the thrust vector produced by the cycloidal rotor. The baseline configuration has a six-bladed rotor with a rotation radius of 0.4m and the span of 0.8m. The phase angle of eccentricity is set to be 10° since the magnitude of the thrust vector has maximum value at that angle setting from the results of experimental tests.

Fig. 22 shows the resultant thrust generated by cycloidal rotor system as a function of rotating speed for various maximum pitch angles. The figure indicates that the forces increase in the quadratic order as the rotating speed increases at a certain θ_a . The maximum thrust from the test is 4.5kgf at $\theta_a=30^\circ$ under the operating speed of $\Omega=450\text{RPM}$. The more thrust generation is failed due to power limitation. An analytic data was obtained to compare the experimental tests data. The agreement between analytic solutions and experiment data for thrust is excellent for all the cases. Fig. 23 presents power required by the rotor in hovering condition. It can be seen that the power curve increases rapidly as the rotating speed is increased in proportion to the cube of the rotating speed. Comparing analytic results with experimental test data, the correlation is good up to 20° , but it becomes fair-to-poor when the maximum pitch angle is higher than 25° .

The maximum pitch angle of blades affects significantly the rotor performance. The thrust forces are produced by cyclic variation of pitch angles of blades during the rotation. Increase in maximum pitch angle causes the each blade to have higher angle of attack causing the forces to increase. The manner in which cyclic pitch affects the thrust forces when operating at rotating speed of 300, 400, and 500 RPM is shown in Fig. 24. The pitch angles are varied up to 30° . From the figure, it can be seen that the thrust increases almost linearly as the pitch angle increases.

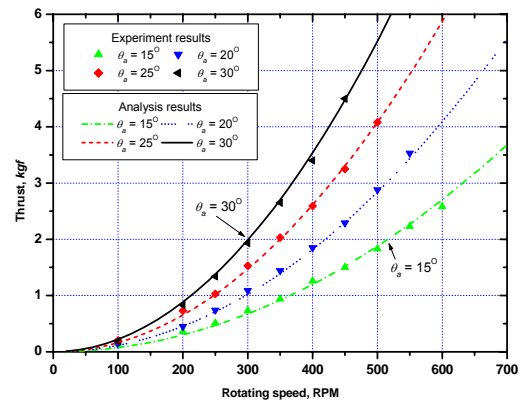


Fig. 22 Thrust variations with respect to the rotating speed for various pitch angles

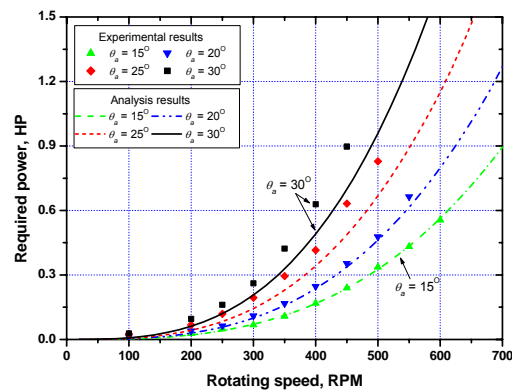


Fig. 23 Power variations with respect to the rotating speed for various pitch angles

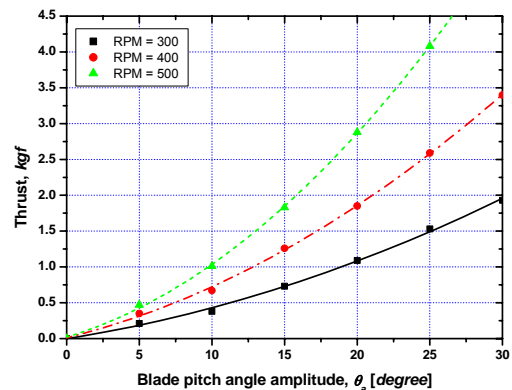


Fig. 24 Effects of the blade pitch angle amplitude on the thrust

In conventional wings operating in air, stall phenomenon would occur if the pitch angle reaches near 30° so that the thrust would be decreased above the stall angle of attack. However, the tendency of decreasing thrust was not observed during the tests. When the blade exceeded the static stall angle and the effective angle of attack changes rapidly, dynamic stall can happen. In general, dynamic stall will occur on any airfoil or other surface when it is subjected to time dependent pitching or plunging motion that takes the effective angle of attack above its normal static stall angle [12]. In the dynamic stall condition, the aerodynamic lift increases. Therefore, the high pitch angle can induce the more thrust. However, the drag is increased dramatically due to the dynamic stall so that power is increased rapidly.

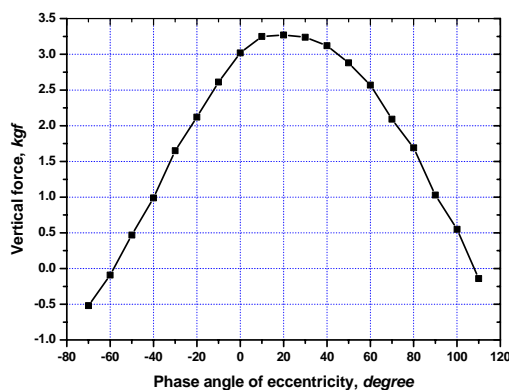


Fig. 25 Effects of the phase angle of the eccentricity on the thrust direction

The cycloidal rotor system has a capability of changing the thrust direction instantly by rotating the phase angle of eccentricity. An additional test for the baseline configuration is made at constant rotating speed and eccentricity in which the phase angle is changed successively by 10° steps from -70° to 110° . Fig. 25 shows the vertical force as a function of phase angle of eccentricity, ε , from -70° to 110° at rotating speed of 450 RPM and maximum blade pitch angle of 25° . The vertical force reaches maximum at a value between 10° to 20° and decreases as the phase angle of eccentricity is apart from the value of phase angle where maximum vertical force is generated. The thrust in vertical direction disappears and thrust is generated only in horizontal direction at about -60° and 110° with the magnitude of thrust kept constant. The horizontal force is not zero during the tests despite the fact that the phase angle is set to be zero. The resultant force is inclined about 20° from the desired direction when the pitch angle θ_a is 25° . The horizontal component of the resultant thrust may be qualitatively explained as a

Magnus effect upon the rotor shaft because the rotor force would generate an induced velocity of appreciable magnitude in the interior of the rotor[17]. The refraction of the induced flow in the downstream part of the rotor is induced by the inner flow, which increases the resultant velocity on a blade in the right side, on the other hand decreases the resultant velocity in the left side. This non-symmetric flows cause the total thrust to be tilted.

The effects of rotor rotating speed on the efficiency as a function of thrust level for the rotor with 6 blades and rotating radius of 0.4 m were examined. Rotating speed kept constant, thrust can be increased by increasing the blade pitch angle. The results from the tests show that the difference of efficiency for the different rotating speeds is little in high thrust levels while better the efficiency, lower the rotating speed in low thrust levels. And since a high rotating speed causes the blades to experience high centrifugal force proportional to the square of the rotating speed, the weight of blades must be increased to resist the forces. Therefore, operation at lower rotating speed is desirable to maximize hovering performance.

Effect of the rotor radius

Figs. 26, 27, and 28 present the influence of the rotor radius on the performance of the rotor. Fig. 26 and Fig. 27 show the thrust variation with respect to rotating speed of rotor with a six-bladed rotor, with radii being 0.45 m and 0.5 m, respectively. In the case of radius 0.4 m, the results are illustrated in the Fig. 22. Comparing Figs. 22, 26 and 27, it can be seen that thrust level also becomes high with larger rotor radius. Examining the thrust values tested at 400 RPM and 20° maximum pitch angle, increases of the thrust of the rotors with radii 0.45m and 0.5 m are 58% and 105%, respectively. The hover efficiency, thrust produced /power required, which is power loading, is plotted with respect to thrust for the radii of 0.4m, 0.45m, and 0.5m with fixed tip speed of 15.7m/s. In case of the each radius, the efficiency is decreased with the increase of thrust. It can be seen from the figure that the larger the radius of the rotor, the better efficiency. The thrust produced by a rotor increases with the increase of rotor radius in spite of rotating tip speed kept constant as shown in Fig. 28. Because the solidity decreases as the rotor radius increases, the efficiency will be high for a rotor with low solidity. For the rotor with 0.5m radius, the efficiency approaches 7 kgf/ HP when the thrust of 3.5 kgf is generated. And the power loading for the rotor with the rotor radius of 0.4m approaches the 6 kgf/ HP. The efficiency of cycloidal rotor is quite high, considering efficiency of a conventional helicopter to be 3~4 kgf/ HP. Thus the cycloidal rotors can provide a large amount of lift for a relatively low power.

Therefore, the aircraft with cycloidal rotor can be an efficiency aircraft in hover compared to helicopter and other vertical takeoff and landing aircraft. Fig. 29 shows these results.

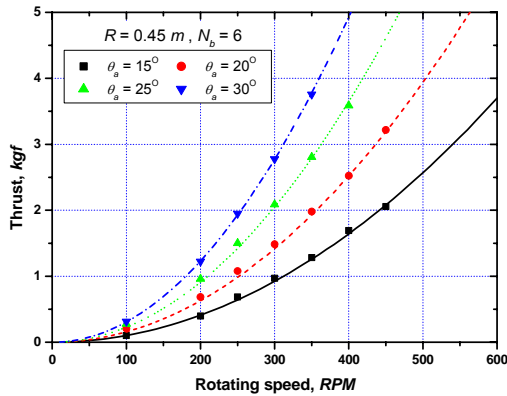


Fig. 26 Thrust variations with respect to the rotating speed for a six-bladed rotor with a rotating radius of 0.45 m

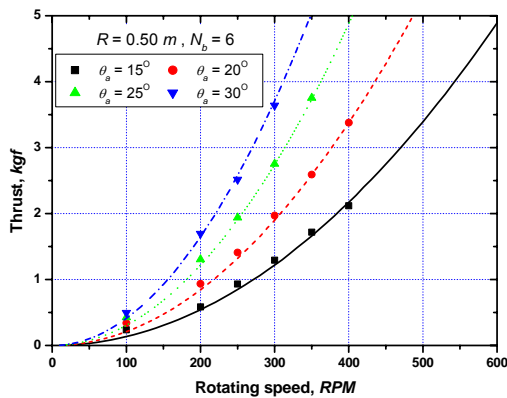


Fig. 27 Thrust variations with respect to the rotating speed for a six-bladed rotor with a rotating radius of 0.50 m

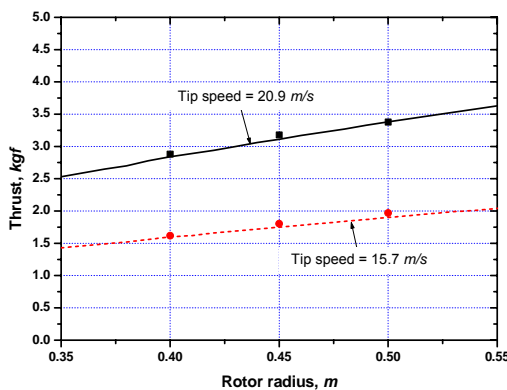


Fig. 28 Effect of the rotor radius on the thrust for a rotor with fixed tip speeds

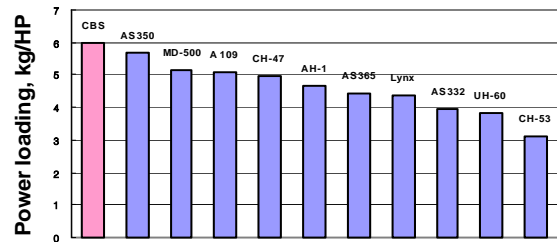


Fig. 29 Hovering efficiency comparison for various helicopters and cycloidal blades system

Effect of the number of blades

Fig. 30 shows the effect of number of blades on the performance of rotor with various radii. Thrust by rotor with 2 blades is smaller than that with 3 blades under the same operating condition. As expected, thrust increases as the number of blades increases. The difference of thrust between 2 blades and 3 blades is relatively large compared to the difference between 3 blades and 6 blades. The rotor with 2 blades can produce thrust only around the blade positions of $\psi = 90^\circ$ and 180° , while the forces produced at the other positions contribute little to the total thrust. In the tests for 2 blades, it was observed that the vibration was severe since periodic impulse was generated by the rotating blades. Among the three cases of number of blades, efficiency of the rotor with 3 blades is higher than with 2 blades and that with 6 blades being the lowest. If the number of blades in rotor increases, the profile-drag power of blades is increased. Thus the efficiency decreases for the 6 blades. Thrust value in the case of rotor with 2 blades is smaller than that with 3 blades. Therefore, in the case with 2 blades, the rotating speed must increase to approach same thrust as with 3 blades. Although the number of blades decreases to 2 blades, the power required increases more since the power is proportional to the cube of the rotating speed. Thus the efficiency of the rotor with 2 blades is lower than that of the rotor with 3 blades. Fig. 30 shows the effects of the rotor radius on the thrust for the rotor with the numbers of blades of 2, 3, 4, and 6 for the fixed rotating speed of 400RPM and $\theta_a = 20^\circ$. The relation between the thrust and radius for the four-bladed rotor is obtained by analytic analysis. The thrust increases more rapidly for a rotor with more blades as the radius increases. The thrust does not increase linearly as the number of blade increases since the direction of local thrust vector with respect to azimuth angle is continuously changed during the rotation of rotor. In the figure, the thrusts produced by the two-bladed, four-blades, and six-bladed rotors with a radius of 0.5m are 2.11 kgf, 2.87 kgf, and 3.38 kgf,

respectively. If the rotor with two blades is attached to additional two blades so that the number of blades becomes four, the thrust increases by an amount of 0.76 *kgf*. Again, adding the two blades to the four-bladed rotor, the thrust increases by an amount of 0.51 *kgf*, not 0.76 *kgf*. Therefore, a rotor with many numbers of blades may be bad for performance since the profile power increases as adding blades to the rotor.

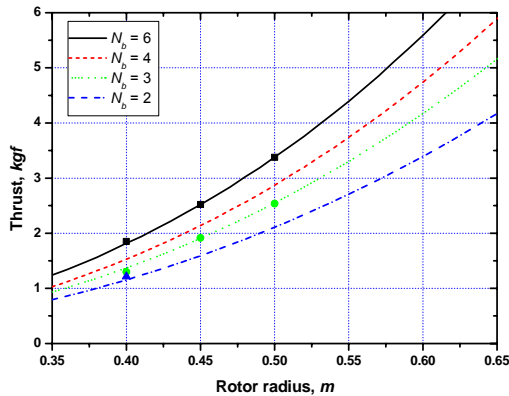


Fig. 30 Effect of the rotor radius on the thrust for a rotor with different number of blades

DEVELOPMENT OF UNMANNED CYCLOCOPTER

In this section, based on the research for cycloidal blades system, the Unmanned Aerial Vehicle(UAV) cyclocopter with cycloidal blades system is designed and developed to evaluate the potential of cycloidal blades system for VTOL vehicle. The development of the cyclocopter is primarily focused on the hovering and low speed forward flight performance. The thrust and power are estimated to use the aerodynamic model in the previous section and CFD analysis. The design of the cyclocopter will be made by consideration of physical constraint, performance, and vibration problems.

Basic cyclocopter performance

The size of the cyclocopter will be determined to consider an engine power and total weight of vehicle. A design specification for gross weight is fixed about 50kg considering the engine performance and cycloidal rotors performance. The dimension of cyclocopter rotor is obtained through analytic analysis and optimization process.

Rotor configuration

Our concept design consists of two rotors rotating each side of a main fuselage. Fig. 31 shows the conceptual design of the UAV cyclocopter capable of vertical take-off and landing. The cyclocopter is composed of two main rotors rotating rotor axis with same direction. The rotor axis is arranged perpendicular to the fuselage in a spanwise direction.

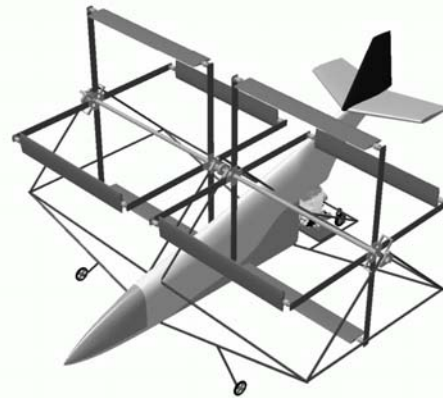


Fig. 31 Conceptual design of UAV cyclocopter

The rotor is supported at both its root and its tip to overcome centrifugal forces and to reduce the vibration problems. The advantage to such arrangement is structurally safe. The feathering system with hinge mechanism is adopted to reduce the loadings on the blades and hub arms. This approach also reduces material required to build the blades and the hubs, and therefore can save the total weight. The method for rotor torque compensation is to place the cyclocopter center of gravity sufficiently below and after the rotor axis so that the reaction couple between the rotor thrust and aircraft weight will cause the aircraft to seek an offset equilibrium trim position.

The rotor is the most important component of the cyclocopter. Proper design of the rotor is critical to meet the performance specification for the cyclocopter. The performance of the cyclocopter rotor depends on the rotor sizing, blade planform and airfoil section. Therefore, the rotor size and rotation speed must be determined to produce the required thrust at given engine power. And the generated torque also must be known to absorb the torque due to rotor rotation. The basic size of cyclocopter rotor is obtained through iteration process. The design parameters of the rotor are rotation speed, span, rotor diameter, chord, number of blades, and airfoil section.

Through several iterations cyclocopter rotor properties are determined like table 2. Thrust and

corresponding power required with respect to rotating speed with increasing the pitch angle amplitude are shown at Figs. 32 and 33.

Table 2 Cyclocopter rotor properties

| Parameter | Value |
|--------------------------|-----------|
| Rotating Speed, Ω | 550 RPM |
| Radius, R | 0.7 m |
| Chord, c | 0.15 m |
| Span, s | 1.0 m |
| Number of blades, N_b | 4 |
| Airfoil section | NACA 0012 |

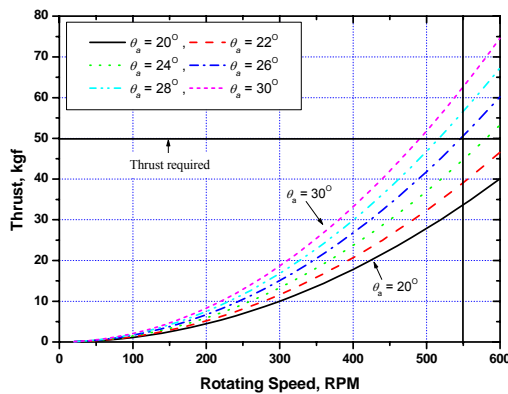


Fig. 32 Thrust with respect to rotating speed with increasing the pitch angle amplitude

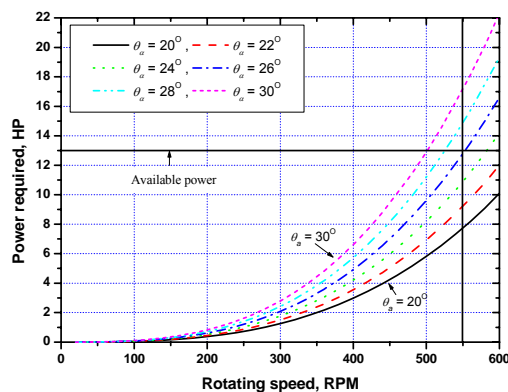


Fig. 33 Power required with respect to rotating speed with increasing the pitch angle amplitude

Thrust and power

The cyclocopter rotor designed is a four-bladed rotor with a diameter of 1.4 m. Rotor geometric and operational properties are listed in Table 2. Figs. 32 and 33 show the thrust produced and corresponding power required as a function of rotating speed for various pitch angle amplitude. Thrust value reaches 50 kgf at the rotating speed of 550 RPM and amplitude of pitch angle of 26° and corresponding power is about 13 horsepower. The available power obtained from the engine is assumed to be approximately 13 HP considering the transmission loss and hub assembly losses though the maximum engine power is 16 HP. For the cyclocopter with the gross weight of 45 kgf, the cyclocopter can take-off vertically when the pitch angle is set to be the 24° . At that condition, the consumed power is about 11 HP.

Main rotor and hub design

The blades are subjected to aerodynamic loadings and centrifugal loadings which is proportional to square of the rotating speed. In contrast to helicopter rotor blades, the cycloidal rotor blades are loaded in the transverse direction of the span so that the bending moment of the blade is critical. Therefore, rotor blades are designed to withstand relatively high transverse centrifugal loadings, supporting components of the cyclocopter weight and responding to a number of aerodynamic harmonic vibratory forcing frequencies.

Blade

The rotor blade is supported at both its root and its tip to overcome centrifugal forces and the vibration problems. The root and tip of the blade are connected to hub arm by means of hinges to reduce the loadings on the blades and hub arms. The hinges allow each blade to deflect in the flap-wise and lag-wise direction under the action of varying aerodynamic forces and centrifugal force. The mechanical hinges are provided on each blade along with a pitch bearing. The hinges are coincident with the pitch bearing through a rod-end bearing which allows the shaft in the bearing to freely tilt in any direction and to rotate.

The blade is mainly deflected due to the centrifugal loading. The large deformation of the blades arises at the center of the span. The deformation deteriorates aerodynamic performance of the rotor and the blade must be designed to prevent the deformation as small as possible, to sustain the centrifugal loadings, and to be light-weighted.

According to the rotor dimension in the Table 2, the

blades are designed to reduce the weight and increase the strength. The blades are made of composite materials. The blades consist of the skin, spar, and trailing stiffener. The blade structures made of composites are analyzed to verify the strength and deformation by using MSC/NASTRAN. The maximum stress by von mises criteria is 160 MPa, of which value is under the ultimate strength of the carbon composite, and the maximum deflection occurs at the center of the blade with a value of 23.4 mm.

Campbell diagram

During each rotor revolution, the airfoil sections on cycloidal rotor encounter a wide diversity of operating conditions. Varying aerodynamic forces and centrifugal force with respect to azimuth angle may cause the rotor to be under the unexpected resonance with the multiple frequency of rotating speed. The natural frequencies of the rotor system vary with increasing the rotor rotating speed due to centrifugal stiffening effects. The variation of the modal frequency with rotor speed will cause some difficulties in terms of avoiding possible resonant conditions. Here the natural frequency of a rotor blade system, composed of the two hub arms and one blade, will be close to, or indeed equal to, that of the aerodynamic forcing effects. The spoke, pan diagram, or Campbell diagram shown in Fig. 34 allows any possible frequency coalescences to be predicted [18]. It assumes that typical aerodynamic forcing frequencies are multiple of the rotor speed. The diagram is a plot of frequency, as ordinate, against rotor speed, as abscissa.

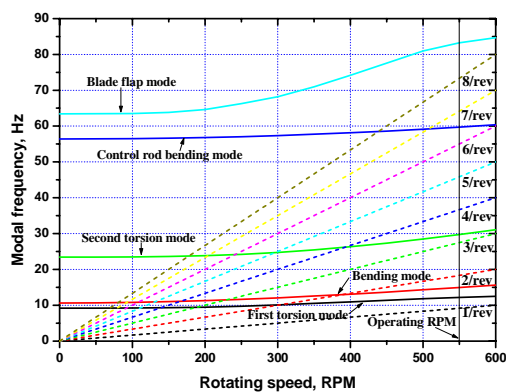


Fig. 34 Rotor modal frequencies as a function of rotating speed

The forcing frequencies appear as straight lines up to 6/rev. and the modal frequency variation can also be plotted. Clearly these must be avoided near to the

operating rotor speed. Crossing of the two frequency plots indicate possible resonant conditions. The 1/rev does not coalesce to all the vibration modes. It is seen crossing of the 2/rev and first torsion mode at 300 RPM. The bending mode meets 2/rev at about 380 RPM. None of modes cross the operating rotating speed, 550 RPM. Therefore, the rotor system is designed to avoid possible dynamic instabilities.

Control mechanism

In order to apply the control mechanism to UAV cyclocopter, the servo motors which are controlled by the radio control system are required to change the magnitude and direction of the thrust vector. The control force must be found to determine the capacity of the servo motors and design the control linkages system. The longitudinal force controls the magnitude of the eccentricity and the transverse force is in charge of the phase angle of the eccentricity. The total control force and torque required for the thrust control of the cyclocopter is obtained by summing up the individual contribution to acting on the eccentricity point of each pitch link. Maximum force occurs about $\psi=0^\circ$ and $\psi=90^\circ$ with a value of 85 N. The minimum torque applied by servo motor at the control block is about 12 kg-cm. Therefore, the servo motors and servo linkages system must be selected and designed to be operated under the action of control force and torque.

For the control realization of the cyclocopter, control block that is isolated from vibration of blade and screw-net mechanism are used. Fig. 35 shows schematic drawing of the control system.

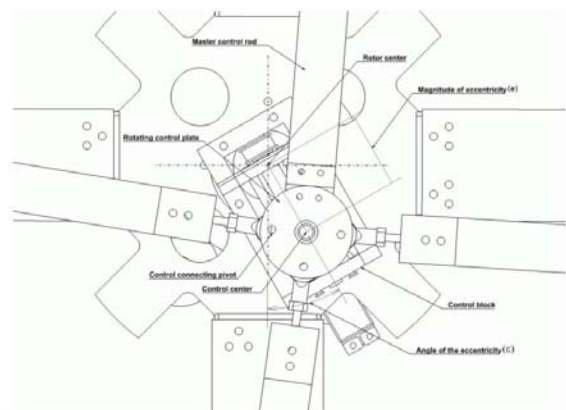


Fig. 35 Schematic drawing of control system

Engine and transmission

Engine selection is important to design the cyclocopter since the cycloidal rotor sizing and

performance can be determined according to given engine power and weight. The kind of engine to be selected depends on the engine's weight, the shaft horse power produced by the engine, and cost. After examining the existing engines producing about 10~20 horse power, IAME K71 engine is selected for powering system of cyclocopter originally designed for the powering of karts.

The dry weight of engine selected is 13.6 kgf and the installed weight except transmission parts is 17 kgf. The engine produces the maximum power of 16.2 HP at running of 10,500 RPM and is allowed to run up to 15,500 RPM. The engine has a single cylinder using the two stroke principle and the cubic capacity of the cylinder is 100 cc. The engine also has an integrated electric starter and is provided with an automatic dry centrifugal clutch.

Transmissions plays role in the power delivery from the engine to main shaft connected to the rotors. Three stages reduction system is used for the purpose of obtain the nominal blade rotating speed. The sprocket chain is used for first stage reduction step from the engine to sprocket shaft. The one-way clutch bearing is incorporated with the sprocket shaft. In case of engine failure, the engine is mechanically disconnected with the sprocket shaft, and one-way clutch system allows the rotors to auto-rotate. The timing belt is used for the second reduction, and finally gears are used to transmit the engine power to main shaft.

Airframe

Airframe structure is designed to contain components of engine, shaft, etc., to withstand ground and flight loads and to withstand the vibratory loadings induced by the rotor. It is evitable that rotors will generate vibratory loading and airframe will respond to this loading. In designing airframe, it is important to avoid the mode frequencies to forcing frequencies generated by rotor. The airframe has many different vibration modes, all of which may be excited by rotor vibration. If the frequency of the mode happens to coincide with that of a force input from the rotor, then high vibration levels are likely to be experienced in the airframe. The airframe can be expected to vibrate at the rotor harmonic frequency and at integer multiples of the rotational frequency. A vibration of the frequency of once per revolution may occur due to rotor unbalance. A vibration in the airframe will also occur when each rotor blade is subjected to an aerodynamic forcing of n per revolution. The frequency of this vibration per revolution which is called blade passing frequency, $N_b\Omega$, is equal to the number of blades. The vibrations at the frequencies of plus or minus one

of the number of blades, $(N_b \pm 1)\Omega$, can also be transmitted from the rotor to the airframe. For the cyclocopter with four-bladed rotor, therefore, the forcing with the frequencies of 1Ω , 3Ω , 4Ω , and 5Ω from the rotor blades is dominantly transmitted to the airframe. Hence, the airframe is so designed that the airframe mode frequencies can be separated from the forcing frequency to reduce the vibrations.

The 1st mode is transversely torsional mode of which frequency is 13.6 Hz. The 2nd mode is also torsion mode about rotor axis and the natural frequency is 17.4 Hz. The 3rd and 4th modes frequencies are 25.2 Hz and 28.6 Hz, respectively. For the rotating speed of 550RPM, the 1/rev is equal to 9.17 Hz. The 2/rev, 3/rev, 4/rev, and 5/rev correspond to 18.3 Hz, 27.5 Hz, 36.7 Hz, and 45.8 Hz, respectively. The third mode and fourth mode are close to 3/rev frequency. Therefore, the vibrations of the airframe may occur in some degree at the 2nd and 3rd modes.

Developed cyclocopter

Cyclocopter is designed to be capable of lifting 50kg weight including pay loads. The designed weight of cyclocopter is 43kg except the pay loads. In this design, the engine weight is too heavy relative to total weight. If the engine is used to be light weight such as rotary engine, the performance of the cyclocopter would be improved. The center of gravity is located at the 50 cm below in the vertical direction and the 34 cm after in the horizontal direction from the rotor axis. This placement of the center of gravity guarantees the cyclocopter to have static stability for the anti-torque problem without addition torque compensation device.

The longitudinal stability of the cyclocopter depends on the torque of the rotor. It is difficult to exactly estimate the torque produced by the rotor. Therefore, it is necessary to find the pitch of the cyclocopter to be either nose-down or nose-up depending on the torque and position of c.g.. The trim angle of the cyclocopter can be calculated in terms of the torque and c.g. offset. The trim angles vary within about 5 degree over all the range of c.g. offset. At the c.g. offset of 0.34 m and the torque value of 150 Nm, the trim angle is zero so that the cyclocopter can hover maintaining the position without nose-down or nose-up.

The assembled cyclocopter is shown in Fig. 36. The longitudinal and lateral lengths of the cyclocopter are 1.65 m and 2.7 m.



Fig. 36 Assembled cyclocopter

CONCLUSIONS

In this paper, the research for cycloidal blades system and cyclocopter installed it was carried out. In order to examine the characteristics and performance of cycloidal blades system, analytical model to predict the thrust and power was developed by using momentum theory and blade element theory. In the aerodynamic model for the cycloidal blades system, the modified blade element momentum theory is applied to the upstream half and downstream half of the cycloidal blades system. The virtual camber effect due to the blade rotation and unsteady aerodynamic effect resulting from the pitching oscillation of blades are also involved in the analysis. The virtual camber effect which arises from the rotating blade subject to a curvilinear flow significantly affects the aerodynamic characteristics.

The performance of the cycloidal blades system is experimentally verified. The sinusoidal low pitch system for control of magnitude and direction of thrust is designed and set up in the test apparatus to obtain high efficiency in hovering state. The experiment tests show that the cycloidal rotor can produce the thrust in any direction in the rotation plane and the rotor has hovering capability as well as forward flight capability. The measured data are also compared to results obtained from analytical approach. The newly developed theory agrees well with experimental results in thrust prediction. However, comparing analytic results with experimental test data for power, the correlation is good in the low amplitude of pitch angle, but it becomes fair-to-poor when the maximum pitch angles are high. The effects of the radius of the rotor, the number of blades, and rotor tip speed on the performance are examined. The hover efficiency in terms of power loading increases as the radius of the rotor increases at a fixed tip speed. In the influence of

number of blades on the rotor efficiency, efficiency of the rotor with 3 blades is higher than that with 2 blades and with 6 blades. The hovering efficiency of the cycloidal rotor is compared to that of helicopter rotors in terms of the thrust produced per unit power required. The efficiency of cycloidal rotor is quite high, considering efficiency of a conventional helicopter. Therefore, the aircraft with cycloidal rotor can be an efficient aircraft in hover compared to helicopter and other vertical takeoff and landing aircraft.

UAV cyclocopter capable of vertical take-off and landing is designed and manufactured to show that cycloidal blades system can become the alternative to an aerial vehicle capable of vertical take-off and landing. The rotor system are designed to withstand relatively high transverse centrifugal loadings and to avoid possible resonance conditions with aerodynamic forcing, and airframe structure is designed to withstand the vibratory loadings induced by the rotor. Cyclocopter is designed to be capable of lifting 50kg weight including pay loads. The designed weight of cyclocopter is 43kg except the pay loads. In order to compensate the rotor torque, the center of gravity is located at the 50 cm below in the vertical direction and the 34 cm after in the horizontal direction from the rotor axis.

From the research for the cycloidal blades system and design of the cyclocopter, it can be concluded that the cycloidal blades system can be used as powerful thrust system capable of easy vector thrusting, and the efficiencies for the aircraft with cycloidal rotor may compare favorably with values for other vertical takeoff and landing aircraft.

ACKNOWLEDGEMENT

The authors acknowledge the partial financial supports of Ministry of Science and Technology by National Research Laboratory program (Contract No. 00-N-NL-01-C-026) and the Brain Korea 21 Project in 2004.

REFERENCE

1. David R. Oliver and Arthur L. Money, "Unmanned Aerial Vehicles Roadmaps 2000-2025," Office of the Secretary of Defense, 2001.
2. Kenneth Munson, Jane's Unmanned Aerial Vehicles and Targets, Jane's Information Group Inc, May 2003.
3. Frederick Kurt Kirsten, "Cycloidal propulsion in air," Bulletin No. 79, Engineering Experiment Station Series, University of Washington, March 1935.
4. Frederick Kurt Kirsten, "Cycloidal Propulsion Applied to Aircraft," Transactions of the American Society of Mechanical Engineers, Vol. 50, No. AER-50-12, pp.25-47, 1928.

5. Fred S. Eastman, "The Full-Feathering Cyclogiro," UWAL Report No. 317, University of Washington Aeronautical Laboratory, Seattle, Washington, March, 1951.
6. Eastman, Fred, Burkheimer, George, and Cotter, W.E., "Wind Tunnel Tests on a High Pitch Cyclogiro," UWAL Report No. 191-A, University of Washington Aeronautical Laboratory, Seattle, Washington, June 2, 1943.
7. John B. Wheatley, "Simplified Aerodynamic Analysis of the Cyclogiro Rotating-wing System," Technical Notes NACA No.467, August 1933.
8. John B. Wheatley and Ray Windler, "Wind-tunnel Tests of a Cyclogiro Rotor," Technical Notes NACA No.528, May 1935.
9. Strickland, J.H., "The Darrieus Turbine: A Performance Prediction Model Using Multiple Streamtubes," Sandia National Laboratories, Albuquerque, NM, SAND75-0431, Oct. 1975.
10. Paraschivoiu, I., "Aerodynamic Loads and Performance of the Darrieus Rotor," Journal of Energy, Vol. 6, No. 6, pp. 406-412, November-December 1982.
11. Paraschivoiu, I. and Delclaux, F., "Double-Multiple Streamtube Model with Recent Improvements," Journal of Energy, Vol. 7, pp. 250-255, May-June 1983.
12. J. Gordon Leishman, Principles of Helicopter Aerodynamics, Cambridge University Press, 2000.
13. Migliore, P. G., Wolfe, W. P., and Fanucci, J. B., "Flow Curvature Effects on Darrieus Turbine Blade Aerodynamics," Journal of Energy, Vol. 4, No. 2, pp. 49-55, March-April 1980.
14. D.S. Kim, "Numerical Performance Analysis of the Cycloidal Blades System," Master' thesis, Seoul National University, 2003.
15. C.Y.Yun, "A New Vertical Take-off and Landing Aircraft with Cycloidal Blades System : Cyclocopter", Ph.D thesis, Seoul National University, 2004
16. Seung Jo Kim, Chul Yong Yun, Daesung Kim, Youngha Yoon, and Illkyung Park, "Design and Performance Tests of Cycloidal Propulsion Systems," 44th AIAA/ASME/ASCE/AHS/ASC Structures, Structural Dynamics and Materials Conference, Norfolk, Virginia, USA. 7-10 April, 2003.
17. John B. Wheatley and Ray Windler, "Wind-tunnel Tests of a Cyclogiro Rotor," Technical Notes NACA No.528, May 1935.
18. Simon Newman, The Foundations of Helicopter Flight, Edward Arnold, 1994.
19. James. H. Boschma, "Modern Aviation Applications for Cycloidal Propulsion," AIAA, Aircraft, Technology Integration, and Operations Forum, Los Angeles, CA, 16-18 Oct., 2001.